Effect of the incident wave angle on the performance of a land-based OWC device

Ayrton Alfonso Medina Rodríguez[1], Gregorio Posada Vanegas[2], Beatriz Edith Vega Serratos[2], Alejandro Martínez Flores[1], Edgar Gerardo Mendoza Baldwin[1], Jesús María Blanco Ilzarbe[3], and Rodolfo Silva Casarín[1]

[1] Institute of Engineering, National Autonomous University of Mexico, Circuito Escolar, CP 04510 Mexico City, Mexico,
ayrtonamedinar@gmail.com,
[2] EPOMEX Institute, Autonomus University of Campeche, Av. Héroe de Nacozari 480 CP 24079 Campeche, Mexico,
[3] Department of Energy Engineering, Faculty of Engineering in Bilbao-UPV/EHU, Plaza Ingeniero Torres Quevedo, 1, CP 48013 Bilbao, Spain

Abstract. The majority of experiments on fixed Oscillating Water Column (OWC) systems assume that water waves impact perpendicularly towards the front wall of the device. However, this seldom occurs in practice owing to wave transformation, which occurs when waves interact with shifting bottom profiles that results in wave reflection, refraction and shoaling. The wave angle of incidence is significant because it can alter the performance of the OWC device, particularly the natural period at which the device resonates. Therefore, this work investigates the interaction of directional waves with a fixed land-based Oscillating Water Column (OWC) device. Theoretical and experimental techniques to study the effect of wave direction on the OWC hydrodynamic performance are described. To formulate the mathematical problem for the theoretical approaches, two-dimensional linear wave theory is employed. The conventional eigenfunction expansion method and the Boundary Element Method are employed to solve the boundary value problem. Then, a series of experimental tests under regular wave conditions were carried out in a spectral wave basin to compare and validate the theoretical results. Variations of the hydrodynamic efficiency with the wave angle of incidence are discussed. Analytical and numerical predictions of the resonance frequency for different wave angles of incidence were found to be in good agreement when compared with experimental tests. Results indicate that analytical and numerical techniques can be employed as design tools to estimate the natural frequency of the system when it interacts with oblique regular waves.

Keywords: Oscillating water column, oblique waves, hydrodynamic efficiency, resonant frequency, wave energy

1 Introduction

Over recent years, a broad range of technologies have been developed which, as they are deployed, will contribute to meeting the energy demands of the world's rapidly growing population, while reducing the consequences associated with the use of fossil fuels. This renewable energy source has attracted the curiosity of numerous inventors, who have proposed a diverse variety of wave extraction devices, with over a thousand wave energy patents to date [1]. Among the several suggested technologies, the OWC device has been shown to be one of the most promising methods for transforming ocean wave energy.

The OWC device is a unique wave energy converter (WEC) system, as it has just two major components: a partially submerged collecting chamber and a power take-off (PTO) mechanism that is placed above sea level. The basic working concept is that the water column inside the collecting chamber oscillates vertically, owing to wave action, forcing the confined air volume back and forth through a turbine connected to a generator [2]. The OWC has many design variations (shore-mounted, sea-bed, and floating systems) allowing it to be deployed at onshore, nearshore and offshore sites.

Despite these advantages, one of the most significant challenges with this type of WEC is its technically sophisticated hydrodynamic mechanism, which involves very complex diffraction and radiation wave processes [1]. A large part of the work on OWC systems published in the last three decades has been on theoretical hydrodynamics, particularly the wave-structure interaction, under the assumption that wave fronts travel normally towards the device [3–7]. However, under real sea circumstances, the wave direction is not always perpendicular to the transverse axis of the OWC chamber [8].

Previous studies have investigated the influence of the wave direction on the hydrodynamic performance of fixed OWC devices with the aid of analytical, experimental and numerical techniques [8–15]. The effects of wave direction on the performance of the OWC chamber were investigated by [8]. Experiments were conducted in a three-dimensional wave basin for distinct wave directions that include the effect of the turbine through a hole in the physical model chamber. They found that, at a large angle of incidence of the wave front with the device, the wave direction had a negligible effect on relative wave height, and the operational performance of the fixed OWC system declined as the incident wave angle decreased.

Through experimental tests, Ashlin et al. [11] studied the performance of an array of OWC devices coupled with an offshore detached breakwater subjected to oblique wave incidence. They observed that when the wave angle drops, the performance of the system declines because the wavefront strikes the system at different times but the natural frequency of the system stays constant. Medina Rodríguez et al. [13] used the matched eigenfunction expansion method and the Boundary Element Method (BEM) to investigate the interaction of oblique water waves with a land-fixed OWC device. They came to the conclusion that increasing the wave direction results in a wider hydrodynamic efficiency band as well as a higher wave frequency at which resonance occurs.

Although there have been several studies on the hydrodynamic performance of land-based OWC systems, the majority of research has concentrated on the two-dimensional interaction of water waves with land-fixed OWC devices. OWC devices are intended to serve as terminator devices (with their major axis perpendicular to the prevailing wave direction in order to capture the most energy) but this seldom occurs in practice. For example, incident water waves impacting the Mutriku Wave Energy Plant [16] are often oblique [17]. In this work, the analytical and numerical techniques employed by [14] are compared with the experimental results obtained for a scaled thick front wall OWC device in a directional wave basin. To complement previous research on land-based OWCs, the goals of this work are to focus on the suitability of theoretical approaches to estimate the natural frequency of a fixed OWC system and the influence of incident wave direction on the hydrodynamic performance by employing different techniques.

2 Mathematical approach

Figure 1 shows the OWC device and the Cartesian coordinate system. The origin is located on the undisturbed free surface and the water depth is defined as h. The waves come from x direction towards the land-based OWC device at an angle θ with the $x-$axis. The OWC consists of a surface-piercing wall at $x = b$, with submergence a and thickness w, and a rigid vertical wall located at $x = 0$. The confined air inside the chamber is assumed to be linked to the atmosphere through a turbine. Only the two-dimensional case is considered, therefore the OWC is assumed to be infinitely long and parallel to the incoming wave crest. The thick-front wall is defined as $B_b = \{(x, z) : (x = b, -a \leq z \leq 0) \cup (b < x < f_w, z = -h_a) \cup (x = f_w, -a \leq z \leq 0)\}$ with $f_w = b + w$, the rigid vertical wall by $B_w = \{(x, z) : x = 0, -h < z < 0\}$, the internal free surface inside the chamber by $F_i = \{(x, z) : 0 \leq x \leq b, z = 0\}$, the external free surface by $F_f = \{(x, z) : f_w \leq x \leq \infty, z = 0\}$, the horizontal bottom by $B_d = \{(x, z) : (0 < x < \infty, z = -h)\}$, while the height of the gap below the front wall by $B_g = \{(x, z) : x = b, -h \leq z \leq -a\}$.

The seawater is assumed inviscid and incompressible, and the wave motion is irrotational. The linearized wave theory is considered to adequately represent the wave motion with the surface tension effects ignored; thus potential theory is used. A velocity potential $\Phi(x, z, t) = \mathrm{Re}\{\phi(x, z)\mathrm{e}^{-\mathrm{i}\omega t+\mathrm{i}\kappa y}\}$ is defined, where ω is the angular frequency of the simple harmonic flow, Re{ } denotes the real part of a complex expression, $\beta = k \sin\theta$, k is the wavenumber of the plane wave and t is the time. Under these assumptions, the spatial velocity potential ϕ is governed by the Helmholtz equation defined as

$$\left(\frac{\partial^2}{\partial x^2} + \frac{\partial^2}{\partial z^2} - \beta^2\right)\phi = 0, \tag{1}$$

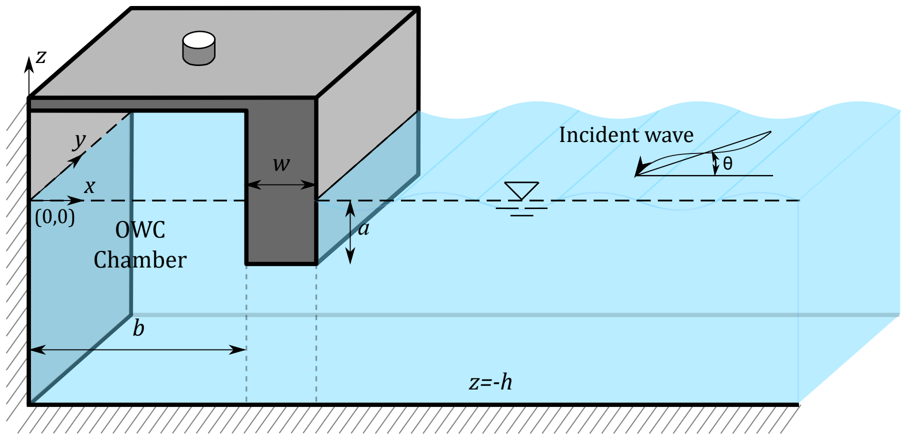

Fig. 1: Definition sketch of the interaction of a land-based OWC device with directional waves.

Together with the no-flow boundary conditions applied at the horizontal bottom, the front wall and the left-rigid vertical wall that are defined by

$$\frac{\partial \phi}{\partial n} = 0 \quad \text{on} \quad B_d, \quad B_b \text{ and } B_w, \tag{2}$$

respectively.

On the free surface, the internal and external linearized boundary conditions are given by

$$\frac{\partial \phi}{\partial z} - K\phi = \begin{cases} \frac{\mathrm{i}\omega p}{\rho g} & \text{on} \quad z = 0, \quad 0 < x < b, \\ 0 & \text{on} \quad z = 0, \quad f_w < x < \infty, \end{cases} \tag{3}$$

respectively, where $K = \omega^2/g$, with g being the gravitational constant, p represents the harmonic pressure distribution in the internal free surface while ρ the seawater density.

Following the procedure of [18], the velocity potential is decomposed into a scattered potential ϕ^S and a radiated potential ϕ^R as follows

$$\phi(x, z) = \phi^S + \frac{\mathrm{i}\omega p}{\rho g}\phi^R, \tag{4}$$

where ϕ^S and ϕ^R satisfy Eqs. (1)–(3), with $p = 0$ inside the OWC chamber for ϕ^S; while for ϕ^R Eq. (3) is replaced by

$$\frac{\partial \phi^R}{\partial z} - K\phi^R = 1 \qquad \text{on} \qquad z = 0, \qquad 0 < x < b. \tag{5}$$

The Sommerfeld radiation condition is imposed at the right-hand end ($x \to +\infty$) of the domain as follows

$$\frac{\partial \phi^{D,R}}{\partial x} - \mathrm{i}k\cos\theta\phi^{D,R} = 0 \qquad \text{as} \qquad x \to +\infty, \tag{6}$$

where ϕ^D is the diffracted potential and $\phi^S = \phi^D + \phi^I$ with ϕ^I being the incident potential, while k is the positive real root of the dispersion relation given by

$$\omega^2 = gk\tanh kh. \tag{7}$$

Similar to the decomposition of the velocity potential, the induced volume flux across the internal free surface is separated into scattering and radiation volume fluxes, q^S and q^R, respectively, as follows

$$q = \int_{F_i} \frac{\partial \phi}{\partial z} dx = q^S + \frac{\mathrm{i}\omega p}{\rho g} q^R, \tag{8}$$

and the continuity of volume flux across the internal free surface and the gap below the front wall is ensured by

$$q^{S,R} = \int_{F_i} \frac{\partial \phi^{S,R}}{\partial z} dx = \int_{B_g} \frac{\partial \phi^{S,R}}{\partial x} dz. \tag{9}$$

3 Solution method

3.1 Eigenfunction Expansion Method

The solution procedure based on the matched eigenfunction expansion method (EEM), as described by [14], is used in this work. This method was chosen because of the simple OWC geometry considered in this work, with a separable governing equation (1) and known horizontal and vertical eigenfunctions. For this purpose, the domain is separated into three regions, where Region 1 ($0 \le x \le b, -h \le z \le 0$) defines the fluid inside the OWC chamber; Region 2 ($b \le x \le f_w, -h \le z \le a$) delimits the fluid below the front barrier; and Region 3 ($b \le x < \infty, -h \le z \le 0$) the fluid outside the OWC structure. First, the spatial velocity potentials in the three regions are expanded in terms of the appropriate eigenfunctions. Then, with the aid of the continuity of pressure and horizontal velocity on the lateral sides of Region 2 defined as

$$\phi_- = \phi_+ \quad \text{and} \quad \frac{\partial \phi}{\partial x}_- = \frac{\partial \phi}{\partial x}_+ \quad \text{on} \quad x = b \text{ and } f_w \quad \text{with} \quad -h \le z \le -a. \tag{10}$$

and by exploiting the orthonormality of the vertical eigenfunctions, a linear system of algebraic equations to solve for the unknowns is obtained.

3.2 Boundary Element Method

The BEM is applied to the Helmholtz equation (1), and the solution procedure for the subdomain method is followed as in [14]. This method is an efficient numerical approach that provides reasonably accurate results [6, 13, 19]. The Helmholtz expression (1) is represented by its boundary integral equation as

$$\alpha(X)\phi(X) + \int_{\Gamma} \phi(Y)\frac{\partial\psi(X,Y)}{\partial n_Y} d\Gamma_Y = \int_{\Gamma} \psi(X,Y)\frac{\partial\phi(Y)}{\partial n_Y} d\Gamma_Y, \tag{11}$$

where ϕ and $\partial\phi/\partial n$ are, respectively, the unknown velocity potential and the normal derivative of ϕ with respect to the field point $Y\,(\hat{\varsigma}, \hat{\eta})$ on the boundary Γ; $X\,(x, z)$ is the source point inside the domain Ω; ψ and $\partial\psi/\partial n$ are, respectively, the fundamental solution of Helmholtz equation and its normal derivative at point Y in Γ; and $\alpha = \tau/2\pi$, where τ is the angle in radians between points X and Y [20].

The fundamental solution of Helmholtz equation is defined as

$$\psi = \frac{K_0\,(kr\sin\theta)}{2\pi}, \tag{12}$$

where K_0 is the modified Bessel function of the second kind and zeroth order which satisfies Eq. (1) and $r = \sqrt{(x-\hat{\varsigma})^2 + (z-\hat{\eta})^2}$ is the distance between points X and Y.

On the other hand, for normal incidence ($\theta = 0$), the velocity potential ϕ is governed by the Laplace equation given by

$$\left(\frac{\partial^2}{\partial x^2} + \frac{\partial^2}{\partial z^2}\right)\phi = 0, \tag{13}$$

whose fundamental solution is

$$\psi = \frac{1}{2\pi}\ln r. \tag{14}$$

4 Experimental investigation

4.1 Test facility

The experimental investigation was carried out in the directional spectral wave basin of the Autonomous University of Campeche, Mexico. The wave basin is 15 m long, 9 m wide and 0.8 m deep and is equipped with a snake type wavemaker of 18 piston paddles (50 cm wide each) that operates an active absorption system. An artificial beach at the other end of the basin acts as a passive wave absorber and is made of gravel D_{50} =5.08 cm with an average weight of 54 g. Figure 2 shows the schematic view of the directional wave basin along with the positions of eight wave gauges and the model tested.

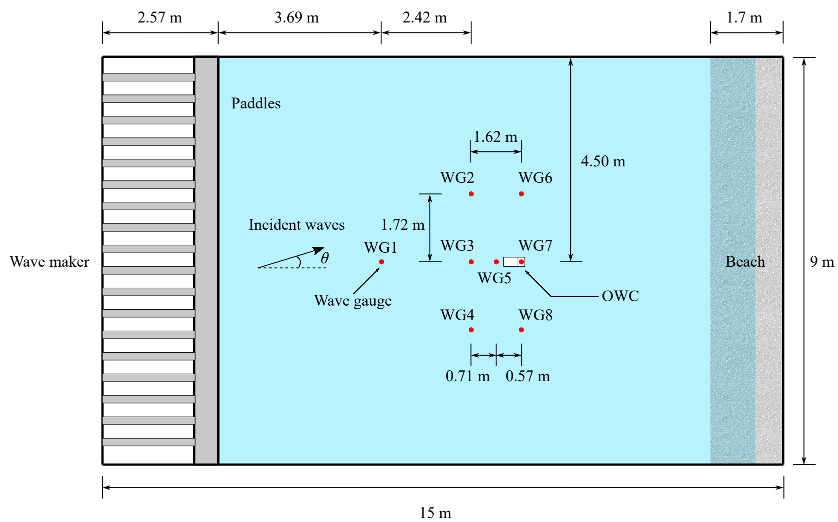

Fig. 2: Schematic plan view of the spectral wave basin and the experimental set-up.

4.2 Test model

The OWC model was built at a 1:20 scale, and operated under the Froude similarity criterion. Froude's similarity was used because it allows the model and full scale to represent an analogous OWC system with the same vertical and horizontal length scales, making them geometrically equal. The scale ratio ($\Lambda = 20$) was determined by the size of the experimental facilities as well as the wave conditions under consideration. However, when applying Froude similarity, other force-to-force ratios, such as inertia to surface tension, inertia to viscosity, and inertia to compressive forces, are distorted [21–23].

Figures 3a shows the dimensional details of the OWC model. The dimensions are based on a single OWC chamber of the Mutriku Wave Energy Plant [14]. The OWC model has the following dimensions: length $b = 155$ mm, width $d = 225$ mm, height $L_1 = 655$ mm, front wall draft $a = 260$ mm and thickness $w = 333$ mm. The gap (B_g) below the thick wall was 140 mm. The OWC model was made using acrylic sheets, 12 mm tihck, that were cut with a laser system. The water depth, $h = 400$ mm, was kept constant throughout all the experiments. Five extra weights (8 kg), made of lead, were used to assure the stability of the OWC device. A distance of 3.0 m between the beach and the OWC model was fixed during the experiments Figs. 3b. The PTO unit acting on the OWC system in this investigation was an impulse turbine. The PTO was simulated by a circular orifice to apply the equivalent resistance of a self-rectifying impulse turbine [23]. The opening ratio of the air hole area to the waterplane area of the OWC chamber (χ) was 0.68%. Previous research has found that OWC models operate best when the orifice area is roughly 1% of the cross-sectional area of

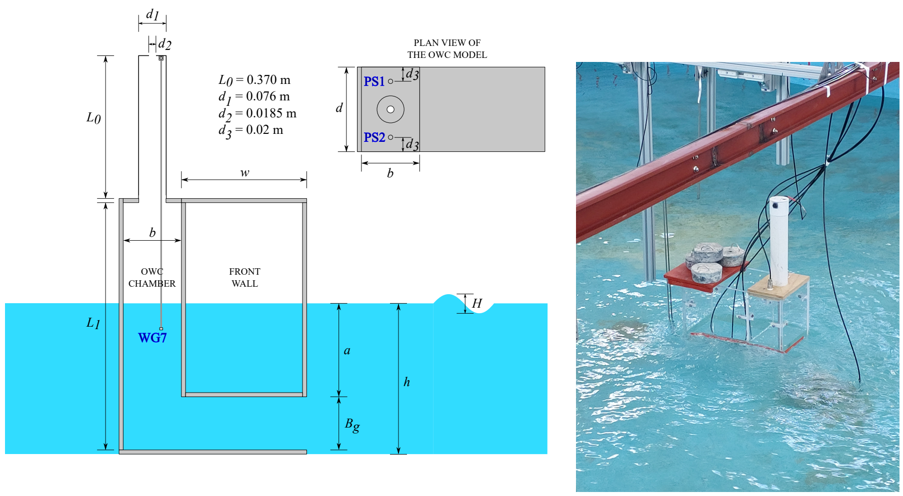

(a) Cross section: details of OWC device.

(b) The experimental set-up of the OWC model.

Fig. 3: Dimensions of the OWC model and set-up in the wave basin.

the chamber. Ashlin et al. [24] found that the optimum energy absorption occurs when the orifice area is roughly 0.68 percent of the OWC chamber; hence, this ratio was chosen, and it was kept constant throughout the experiments.

4.3 Instrumentation

The water-free surface elevations outside the OWC model were recorded by seven resistance type wave gauges installed within the wave basin. Wave gauges 1 to 5 were located in front of the OWC model, and WG6 and WG8 were mounted 1.72 m from the lateral sides of the model, as shown in Fig. 2. One resistance wave gauge (WG7) was installed inside the chamber of the model as well as two air pressure gauge sensors. All of the sensors have a sampling frequency of 100 Hz. The pressure transducers, on the other hand, have a measurement range of 0.3 bar. The power absorbed by the system was calculated using the differential air pressure obtained by PS1 and PS2, as well as the water free surface elevation of the chamber, measured by WG7. The measurements were analysed within the time window of the steady state (i.e., the time-series window without start-up time and reflection).

4.4 Experimental set-up

The OWC device was tested under regular waves. Experimental conditions are summarized in Table 1. The performance of the OWC was studied by varying the wave height, from H =0.02 m to H =0.10 m, in increments of 0.02m (from H =0.04 m to H =2.0 m, in full-scale dimensions); wave period, from T =1.0 s

Table 1: Experimental conditions.

Parameter	Values
Water depth (h)	0.4 m
Incident wave height (H)	0.02–0.10 m at 0.02 m interval
Wave period (T)	1.0–3.0 s at 0.2 s interval
Wave length (λ)	1.464, 1.936, 2.393, 2.836, 3.269, 3.695, 4.115, 4.532, 4.945, 5.356 and 5.765 m

to T =3.0 s, in increments of 0.2 s (from T =4.47 s to T =13.42 s, in full-scale dimensions); and incident wave angle, from θ =0° to θ =30°, in increments of θ =15°.

5 Hydrodynamic efficiency

To evaluate the system performance, the hydrodynamic efficiency was used as

$$\epsilon = \frac{P_{out}}{P_{in}}, \tag{15}$$

where P_{in} is the available power over one wave period of a monochromatic wave given by

$$P_{in} = Ec_g \tag{16}$$

with E being the total energy per wave period and c_g the group velocity given by

$$E = \frac{1}{2}\rho g d \left(\frac{H}{2}\right)^2, \tag{17}$$

$$c_g = \frac{1}{2}\frac{\omega}{k}\left(1 + \frac{2kh}{\sinh(2kh)}\right), \tag{18}$$

respectively, where k represents the wave number that satisfies the dispersion relation given by

$$\omega^2 = gk\tanh(kh), \tag{19}$$

and ω is the angular frequency of the waves.

On the other hand, the average power absorbed from regular waves P_{out} can be determined by the integration of the instantaneous free surface oscillation inside the chamber moving with a velocity (V_{fs}) under the air pressure (ΔP) as follows

$$P_{out} = \frac{1}{T_{fin} - T_{ini}} \int_{T_{ini}}^{T_{fin}} \Delta P S_{chamber} V_{fs} dt, \tag{20}$$

where T_{ini} and T_{fin} are the initial and final times in the steady state region of the measurements; $S_{chamber} = b \times d$ is the water plane area of the OWC chamber; and t is the time. The quantity V_{fs} can be estimated by calculating the first time derivative of the third-order approximation to the free surface elevation inside the OWC chamber [25] as

$$V_{fs} = \frac{2\eta_{j+1} + 3\eta_j - 6\eta_{j-1} + \eta_{j-2}}{6\Delta t}, \tag{21}$$

where η_j is the elevation of free surface at time t_j, j is the current time value and Δt is the sampling interval. Furthermore, the air pressure within the chamber ΔP is determined by averaging the data gathered from the two pressure gauges, PS1 and PS2, at each time instant.

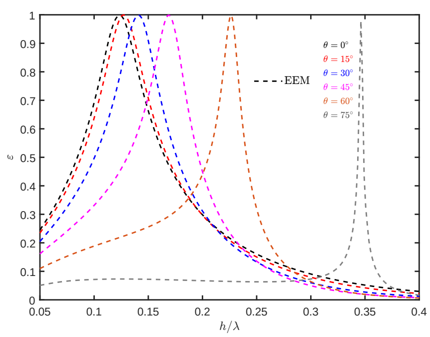

(a) Analytical results obtained by the matched EEM.

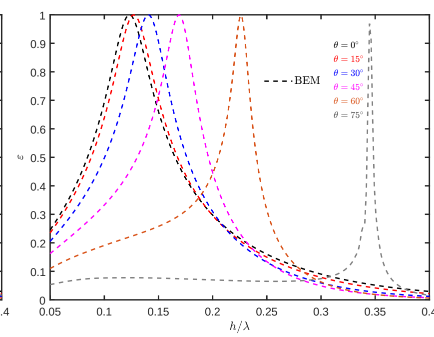

(b) Numerical results obtained by the BEM

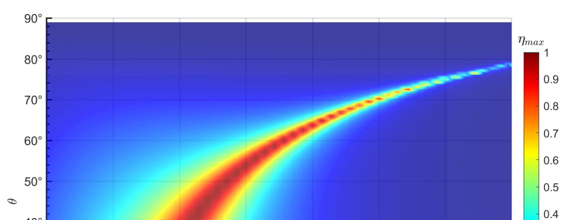

(c) Analytical results of the hydrodynamic efficiency ε as a function of h/λ and θ.

Fig. 4: Hydrodynamic efficiency ε versus h/λ for different wave direction (θ) with $b/h = 0.3875$, $a/h = 0.65$ and $w/h = 0.83125$.

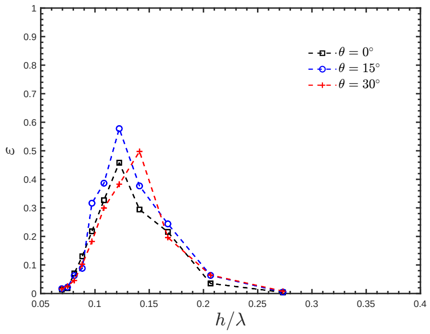

(a) Experimental results for $H/h = 0.05$.

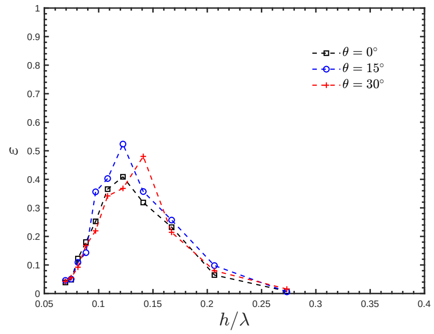

(b) Experimental results for $H/h = 0.10$.

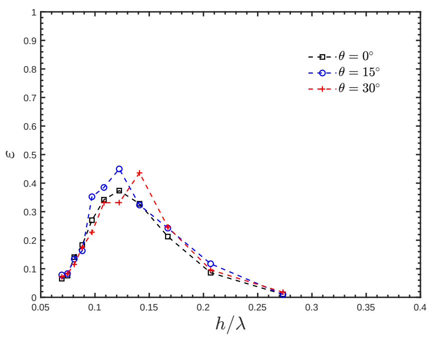

(c) Experimental results for $H/h = 0.15$.

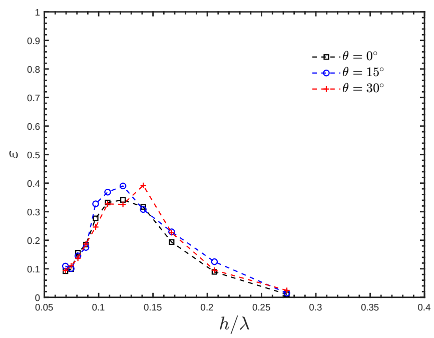

(d) Experimental results for $H/h = 0.20$.

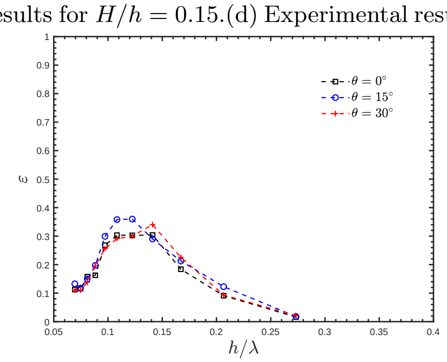

(e) Experimental results for $H/h = 0.25$.

Fig. 5: Hydrodynamic efficiency ε versus h/λ for different wave height to water depth ratios (H/h) and wave direction (θ).

6 Results

In this subsection, the theoretical and experimental results of the land-based OWC device are shown. The chosen values for performing the two-dimensional numerical calculations were $h = 8.0$ m, $a = 5.20$ m, $b = 3.10$ m and $w = 6.65$ m with a wave period T in the range of $2.80 \leq T \leq 30$ s. Thus, the hydrodynamic efficiency ε for different incidence wave angles and wave heights are presented and discussed.

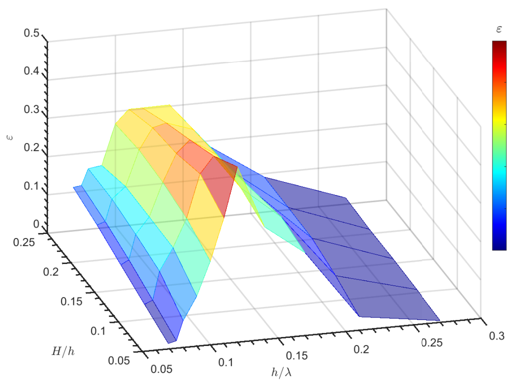

(a) Experimental results for $\theta = 0°$.

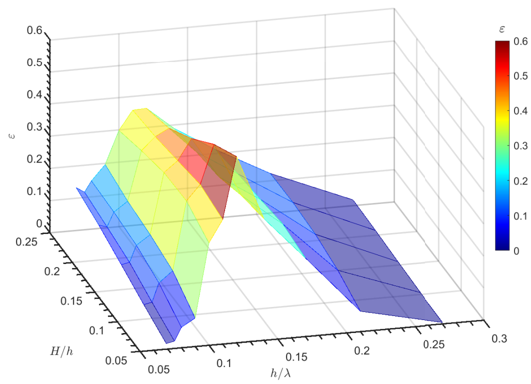

(b) Experimental results for $\theta = 15°$.

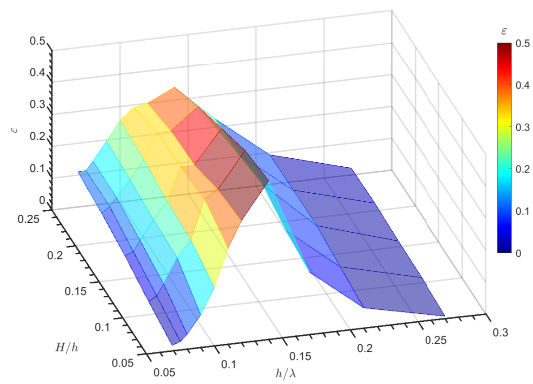

(c) Experimental results for $\theta = 30°$.

Fig. 6: Hydrodynamic efficiency ε as a function of the non-dimensional frequency h/λ and the wave height to water depth ratio H/λ for the three different wave directions.

Figures 4a-4c show the hydrodynamic efficiency ε for different wave angles of incidence versus h/λ obtained by the matched EEM and the BEM. Figures 4a and 4b show that the semi-analytical and numerical findings derived by the EEM and the BEM, respectively, are in good agreement. It is seen in Figs. 4a and 4b that the hydrodynamic efficiency curves for θ =0° and 15° are almost superimposed; however, with the aid of Fig. 4c it is corroborated that the effect of wave direction on the hydrodynamic efficiency is significant for θ beyond 15°. It is also observed that as θ increases, the value of the non-dimensional frequency h/λ at which resonance occurs also increases, while the hydrodynamic efficiency

Table 2: Comparison of theoretical, numerical and experimental h/λ values at which resonance occurs for different wave angles.

	Wave direction					
	0°	**15°**	**30°**	**45°**	**60°**	**75°**
Method	h/λ					
EEM	0.126	0.129	0.143	0.170	0.228	0.348
BEM	0.124	0.129	0.143	0.170	0.227	0.346
Experimental	0.122	0.122	0.141	-	-	-

bandwidth is significantly reduced. From Figs. 4a and 4b, the values of $h/\lambda(= 0.126,\ 0.129,\ 0.143,\ 0.170,\ 0.228$ and $0.348)$ where the maximum value of ε occurs, correspond to wave periods $T(= 7.85,\ 7.70,\ 7.08,\ 6.18,\ 5.02$ and 3.89 s). To make better use of the available wave energy, in practice, this feature of the resonance frequency changing due to the direction of the waves can be useful when deciding to install a land-based OWC device.

From Figs. 5a to 5e show the experimental results for the hydrodynamic efficiency ε versus h/λ for different wave height to water depth ratios and wave angles of incidence. In these figures, as was observed in Figs.4a-4c, it is seen that the value of h/λ at which ε is maximum increases as the wave angle increases. This is better observed for $\theta = 15°$ to $30°$. This pattern is because shorter waves that reach the structure at an oblique angle can excite the system with lesser energy dissipation. It also means that for bigger wave angles, the OWC chamber must interact with shorter wavelengths to resonate. From these figures, it is also observed that wave height does not influence the value of h/λ at which resonance occurs and that the peaks in hydrodynamic efficiency are higher for smaller wave height to water depth ratios.

The hydrodynamic efficiency ε as a function of the non-dimensional frequency h/λ and the wave height to water depth ratio H/h is shown in Figs. 6a-6c. These figures, along with Figs. 5a-5e, show that ε increases when H/h decreases, regardless of the wave direction, and that the hydrodynamic efficiency is significantly reduced for short wavelengths $h/\lambda > 0.20$. Moreover, it can be observed that the values of h/λ where ε is maximum remain unaltered for the H/h ratio.

Finally, Table 2 gives a comparison between the analytical, numerical and experimental techniques of the values of the non-dimensional frequency h/λ at which resonance occurs for different wave directions. The values computed from the theoretical and numerical tools are in accordance with those obtained in the experimental tests. This demonstrates how potential flow-based procedures, such as the matched EEM and BEM, can be used for the initial design of a land-based OWC chamber to resonate for a specific wave period~~,~~ for a particular location, prior to design the entire system. Then, findings can be corroborated by experimental testing of the selected OWC model, under regular and irregular wave conditions.

7 Conclusions

Analytical and numerical methodologies, as well as experimental testing under regular waves, were used to evaluate the performance characteristics of a land-based OWC device exposed to diverse incident wave directions and wave heights. The findings of this study are summarised below:

- The matched EEM and BEM were shown to be appropriate for predicting the resonance frequency of a land-fixed OWC model, with a thick-front wall, when it interacts with regular waves at different angles of incidence. These two methods can be used as an initial means for designing an OWC chamber based on the wave environment of a proposed installation site.
- The resonant frequency of the system increases when the incident wave angle increases. This trend was more visible for wave angles of over $15°$ in both the numerical and experimental techniques.
- Regarding the effect of the wave height, it was observed that this does not affect the value of the resonance frequency. However, the magnitude of the peak in the hydrodynamic efficiency increases when wave height decreases.

Additional numerical and experimental tests with varied OWC chamber designs and incidence wave angles are required to confirm the applicability of the matched EEM and BEM for estimating the resonant frequency of land-fixed OWC systems. Finally, it is hoped that the findings of this study lead to successful wave energy harvesting and motivate further investigation on the interaction of land-based OWC devices with directional waves.

Acknowledgements

The present research has been developed under the framework of CEMIE-Océano (Mexican Centre for Innovation in Ocean Energy). Project FSE-2014-06-249795 financed by CONACYT-SENER- Sustentabilidad Energética.

References

1. Falcão, A.F.O.: Wave energy utilization: A review of the technologies. *Renew. Sustain. Energy Rev.*, *14(3)*, 899-918 (**2010**).
2. Falcão, A.F.O., Henriques, J.C.C.: Oscillating-water-column wave energy converters and air turbines: A review. *Renew. Energy*, *85*, 1391–1424 (**2016**).
3. Evans, D., Porter, R.: Hydrodynamic characteristics of an oscillating water column device. *Appl. Ocean Res. 17*, 155-164 (**1995**).
4. Morris-Thomas, M.T., Irvin, R.J., Thiagarajan, K.P.: An Investigation Into the Hydrodynamic Efficiency of an Oscillating Water Column. *J. Offshore Mech. Arct. 129*, 273–278 (**2006**).
5. Şentürk, U., Özdamar, A.: Wave energy extraction by an oscillating water column with a gap on the fully submerged front wall. *Appl. Ocean Res. 37*, 174–182 (**2012**).

6. Rezanejad, K., Bhattacharjee, J., Guedes Soares, C.: Stepped sea bottom effects on the efficiency of nearshore oscillating water column device. *Ocean Eng. 70*, 25–38 (**2013**).
7. Koley, S., Trivedi, K.: Mathematical modeling of oscillating water column wave energy converter devices over the undulated sea bed. *Eng. Anal. Bound. Elem. 117*, 26–40 (**2020**).
8. Jin, J., Liu, Z., Hyun, B.S., Hong, K.: Effects of wave direction on performance of oscillating water column type wave energy convertor. *Proceedings of the International Offshore and Polar Engineering Conference*, 582–587 (**2012**).
9. Martins-rivas H., Mei C.C.: Wave power extraction from an oscillating water column along a straight coast. *Ocean Eng. 36(6)*, 426-433 (**2009**).
10. Nader J.R., Zhu S.P., Cooper P, Stappenbelt B.: A finite-element study of the efficiency of arrays of oscillating water column wave energy converters. *Ocean Eng. 43*, 72-81 (**2012**).
11. John Ashlin, S., Sannasiraj, S.A., Sundar, V.: Hydrodynamic performance of an array of oscillating water colum device exposed to oblique waves In Proceedings of the 12th International Conference on Hydrodynamics. Egmond aan Zee, The Netherlands, September 2016.
12. Malara G., Gomes R.P.F., Arena F., Henriques J.C.C., Gato L.M.C., Falcão A.F.O.: The influence of three-dimensional effects on the performance of U-type oscillating water column wave energy harvesters *Renew. Energy 111*, 506-522 (**2017**).
13. Medina Rodríguez, A.A., Martínez Flores, A., Blanco Ilzarbe, J.M., Silva Casarín, R.: Interaction of oblique waves with an Oscillating Water Column device. *Ocean Eng. 228*, 108931 (**2021**).
14. Medina Rodríguez, A.A., Silva Casarín, R., Blanco Ilzarbe, J.M.: The influence of oblique waves on the hydrodynamic efficiency of an onshore owc wave energy converter. *Renew. Energy 183*, 687–707 (**2022**).
15. Medina Rodríguez, A.A., Posada Vanegas, G., Silva Casarín, R., Mendoza Baldwin, E.G., Vega Serratos, B.E., Puc Cutz, F.E., Mangas Che, E.A.: Experimental Investigation of the Hydrodynamic Performance of Land-Fixed Nearshore and Onshore Oscillating Water Column Systems with a Thick Front Wall *Energies 15*, 2364 (**2022**). https://doi.org/10.3390/en15072364
16. Torre-Enciso, Y., Ortubia, I., López De Aguileta, L.I., Marqués, J.: Mutriku Wave Power Plant: From the Thinking out to the Reality. In Proceedings of the 8th European Wave and Tidal Energy Conference (EWTEC), Uppsala, Sweden, 7–10 September 2009.
17. Ibarra-Berastegi, G., Sáenz, J., Ulazia, A., Serras, P., Esnaola, G., Garcia-Soto, C.: Electricity production, capacity factor, and plant efficiency index at the Mutriku wave farm (2014–2016). *Ocean Eng. 147*, 20–29 (**2018**).
18. Evans, D.V.: Wave-power absorption by systems of oscillating surface pressure distributions. *J. Fluid Mech. 114*, 481–499 (**1982**).
19. Medina Rodríguez, A.A., Silva Casarín, R., Blanco Ilzarbe, J.M.: A Theoretical Study of the Hydrodynamic Performance of an Asymmetric Fixed-Detached OWC Device. *Water*, *13(19)*, 2637 (**2021**).
20. Katsikadelis, J.: *Boundary Elements. Theory and Applications*; Elsevier: Amsterdam, The Netherlands, 2002.
21. Sarmento, A.J.N.A.: Model-Test Optimization Of An Owc Wave Power Plant. *Int. J. Offshore Polar Eng. 3* (**1993**).
22. Weber, J.: Representation of non-linear aero-thermodynamic effects during small scale physical modelling of oscillating water column wave energy converters. In Pro-

ceedings of the European Wave and Tidal Energy Conference EWTEC, Porto, Portugal, 2007.
23. Falcão, A.F.O., Henriques, J.C.: Model-prototype similarity of oscillating-water-column wave energy converters. *Int. J. Mar. Energy 6*, 18–34 (**2014**).
24. John Ashlin, S., Sundar, V., Sannasiraj, S.: Effects of bottom profile of an oscillating water column device on its hydrodynamic characteristics. *Renew. Energy 96*, 341-353 (**2016**).
25. López, I., Pereiras, B., Castro, F., Iglesias, G.: Performance of owc wave energy converters: Influence of turbine damping and tidal variability. *Int. J. Energy Res 39*, 472-483 (**2015**).